NIH Public Access
Author Manuscript
Proteomics. Author manuscript; available in PMC 2009 September 14.

Published in final edited form as:
Proteomics. 2009 March ; 9(6): 1538–1547. doi:10.1002/pmic.200800528.

NSOM- and AFM-based nanotechnology elucidates nano-structural and atomic-force features of a *Y. pestis* V immunogen-containing particle vaccine capable of eliciting robust response

Gucheng Zeng[1,*], **Jianbo Chen**[1,2,*], **Liyun Zhong**[1,*], **Richard Wang**[1], **Lifang Jiang**[2], **Jiye Cai**[1,3], **Lin Yan**[1], **Dan Huang**[1], **Crystal Y. Chen**[1], and **Zheng W. Chen**[1]

[1] Department of Microbiology and Immunology, University of Illinois, Chicago, IL, USA

[2] Department of Microbiology, Zhongshan Medical College, Sun Yat-Sen University, Guangzhou, P. R. China

[3] Department of Chemistry and Institute for Nano-Chemistry, Jinan University, Guangzhou, P. R. China

Abstract

It is postulated that unique nanoscale proteomic features of immunogen on vaccine particles may determine immunogen-packing density, stability, specificity, and pH-sensitivity on the vaccine particle surface and thus impact the vaccine-elicited immune responses. To test this presumption, we employed near-filed scanning optical microscopy (NSOM)- and atomic force microscopy (AFM)-based nanotechnology to study nano-structural and single-molecule force bases of *Yersinia pestis* (*Y. pestis*) V immunogen fused with protein anchor (V-PA) loaded on gram positive enhancer matrix (GEM) vaccine particles. Surprisingly, the single-molecule sensitive NSOM revealed that ~90% of V-PA immunogen molecules were packed as high-density nanoclusters on GEM particle. AFM-based single-molecule force analyses indicated a highly stable and specific binding between V-PA and GEM at the physiological pH. In contrast, this specific binding was mostly abrogated at the acidic pH equivalent to the biochemical pH in phagolysosomes of antigen-presenting-cells in which immunogen protein is processed for antigen presentation. Intranasal mucosal vaccination of mice with such immunogen loaded on vaccine particles elicited robust antigen-specific immune response. This study indicated that high-density, high-stability, specific, and immunological pH-responsive loading of immunogen nanoclusters on vaccine particles could readily be presented to the immune system for induction of strong antigen-specific immune responses.

Keywords

AFM; Nanobiotechnology; Nanoimmunology; Nanoproteomics; NSOM

1 Introduction

Subunit mucosal vaccines that consist of rationally selected immunogens are extremely attractive for disease prevention due to their superior safety profile and ease of bulk manufacturing by recombinant DNA technology. Considerable effort has been directed toward

Correspondence: Professor Zheng W. Chen, University of Illinois, College of Medicine, 835 S. Wolcott Ave, Chicago, IL 60612, USA, E-mail: zchen@uic.edu, Fax: 1312-996-5725.

*These authors contributed equally to this work.

The authors have declared no conflict of interest.

NIH-PA Author Manuscript
NIH-PA Author Manuscript
NIH-PA Author Manuscript

NIH-PA Author Manuscript

NIH-PA Author Manuscript

NIH-PA Author Manuscript

development of subunit nano- or microparticulated vaccines because vaccine particles loaded with immunogens are recognized as one of the most promising technologies for vaccine development [1]. While progress has been made regarding nano- or micro-vaccine particle delivery system, pH [2], size [3], surface charges [1], biochemical, and immunological aspects, it is not known whether unique nano-organization and molecular force-binding properties in the interface between immunogen and vaccine particles may impact the vaccine-elicited immune response. Given the possibility that nanostructure and single-molecular force bases [4,5] of the vaccine particle may determine immunogen-packing density, stability, specificity, and pH-sensitivity on the vaccine particle surface and thus impact the vaccine-elicited immune responses, it is important to elucidate nanoscale proteomic and atomic force-binding features of an immunogen loaded on vaccine particles. Currently there is no report regarding the nano-structural and single-molecule force bases of an immunogen loaded on vaccine particles.

Here, we utilized a AFM- and NSOM-based nanotechnology to elucidate nano-structural and single-molecule force-binding features of the vaccine particles, in which recombinant *Yersinia pestis* V protein immunogen was loaded on a *Lactococcus lactis*-derived gram positive enhancer matrix (GEM) [6] (Figs. 1A and B). *Y. pestis* V antigen is a key component that mediates the function of the *Yersinia* outer protein virulence factors [7,8]. Since there is no licensed vaccine against plague, development of a safe, effective vaccine against plague is certainly one of the important biodefense counter-measures. The reason why we choose V antigen is that subunit vaccines comprise of *Y. pestis* Vantigen can confer effective immune protections against *Y. pestis* challenge in mice [9]. It is important to note that AFM has emerged as a powerful nanotechnology for studying protein nanostructures [10–12]and single-molecule forces between single proteins [13] or within proteins [14] thanks to its high force and spatial resolution. On the other hand, NSOM has proven to be a useful nanotechnology for the study of protein nanostructures because of its superior optical resolution [15–22]. We have recently developed AFM- and NSOM-based nanotechnology platforms to study molecular interaction [13], molecular [10,11], and cellular [23] nanostructures, and nanoscale *in vivo* immune response of immune molecules [17]. In the current study, NSOM- and AFM-based nanotechnology allowed us to elucidate nano-structural and atomic-force binding features underlying highly dense, stable, specific, but immunological-pH-responsive loading of *Y. pestis* V immunogen on the particle vaccine capable of eliciting robust antigen-specific immune response.

2 Materials and methods

2.1 Bacterial strains and growth conditions, production of the GEM particles, cloning of DNA encoding V antigen into *L. lactis* vector plasmids, preparation of subunit GEM particle vaccine

Please see the Supporting Information for the full materials and methods of this section.

2.2 AFM-based single-molecule force-binding analysis

FPLC-purified V immunogen fused with protein anchor (V-PA) (64.36 kD) and V (38.95 kD) proteins were used for AFM force-distance analyses (please see the Supporting Information for the full details of protein purification). AFM silicon nitride tips (Veeco, CA, USA) were functionalized following the protocol as described in our previous work and Supporting Information [13]. All prepared GEM or *L. lactis* cell PBS suspensions were filtered by Millipore polycarbonate filter membrane with a diameter about 0.8 μm. After filtering of particle or cell suspension, filters holding particles or cells were turned upside down and attached to a steel sample patch by double faced tape. Before performing each force-distance (F-D) experiment, AFM cantilever spring constant was calibrated following instructions of Veeco. Images were performed using functionalized AFM tips in buffers with different

NIH-PA Author Manuscript

NIH-PA Author Manuscript

NIH-PA Author Manuscript

composition as mentioned in the paper in contact mode on an Explorer AFM (Veeco). After localization of individual particles or cells by imaging, AFM F-D curves were obtained on GEM surface. All AFM F-D curves were obtained in the same loading rate and contact time. AFM force-percentage histograms and boxplot were generated by SAS system 8.0 (SAS Institute, NC, USA).

2.3 Confocal microscopy imaging and NSOM-based nanoscale imaging

Please see the Supporting Information for the full details of confocal microscopy imaging. For NSOM-based nanoscale imaging. Briefly, 2% formalin PBS solution was first used to fix GEM or *L. lactis* cells loaded V-PA, V only or heat-shock protein (HSP) 70 (Sigma, MO, USA) control proteins. Monoclonal Anti-c-Myc biotin conjugate (Sigma) were used to label V-PA, followed by QD streptavidin conjugates 655 (~20 nm for the diameter [17], personal communication with Invitrogen scientists) for immune staining. For each labeling step, PBS was applied to wash twice to remove any unbound antibody or QDs. Before NSOM imaging, confocal microscopy was used to monitor that V-PA had been specifically loaded onto GEM as described in Section 2. GEM and *L. lactis* cell PBS suspensions were washed twice by double deionized (DD) water to rule out the influence of salt crystals. And NSOM topographic images also indicated that there were no salt crystals on cover slides after DD water wash. DD water suspension of vaccine particle and *L. lactis* cell was loaded onto cover slides coated with poly-L-lysine (Sigma) for NSOM imaging. GEM were imaged based on an Aurora 3 NSOM system (Veeco) with the single-molecule detection sensitivity, as schematically shown in Fig. S1 of Supporting Information by NSOM probes with an aperture diameter of ~50–80 nm (Veeco). QD-labeled GEMs were excited by using a semiconductor laser (Coherent, USA; cube, 404 nm). The excitation laser (150 W/cm^2) is coupled into an Al-coated tapered fiber probe. The collected laser is filtered with a 650/40 nm bandpass filter and the fluorescence separated into two orthogonal polarization components by a polarizing beam splitting cube (PBS) (400–700 nm, Newport, CA). Finally, the signal is focused onto two avalanche photodiodes (APDs, PerkinElmer, Canada). NSOM images were analyzed by MatLab 7.0. The percent of vertical and horizontal polarization colocalization was calculated as: no. of colocalized spots/no. of horizontal polarization spots + vertical polarization spots. The fluorescent intensity of QDs was calculated as described by the literature [24]. The QD/V-PA = 1:1 binding model was determined based on the estimation that one monocolonal biotin-conjugated anti-Myc antibody should bind one V-PA protein under the saturation condition, and one QD streptavidin counjugate might bind at least one biotin-conjugated anti-Myc antibody.

2.4 Animals, immunization, sample collection, and ELISA of the titer of V immunogen-specific antibody response

Please see the Supporting Information for the full details regarding *in vivo* experiments and ELISA.

2.5 Statistical analysis

The data for the comparison between V-PA-GEM force and gp120-CD4 force and the antibody responses between GEM-V-PA and GEM groups were analyzed by one-way ANOVA for statistical significance as describe previously [25]. The differences between groups were evaluated for statistical significance by calculating the *p*-values.

3 Results and Discussion

3.1 Biochemical characterization of V-PA immunogen loaded on GEM vaccine particles

V immunogen loaded on GEM vaccine particle was developed through two major steps: (i) expression and purification of recombinant V-PA expressed by recombinant *L. lactis* PA1001

NIH-PA Author Manuscript

NIH-PA Author Manuscript

NIH-PA Author Manuscript

expressing V-PA (Figs. 1C and D); (ii) production of GEM particles that were able to bind to a protein anchor (PA) fused with V protein immunogen (Figs. 1A and B). This was done through HCl boiling treatment of food-grade *L. lactis* MG1363 for surface exposure of peptidoglycan capable of binding to PA [6, 26]; thus, GEM particle vaccine loaded with V-PA immunogen was produced by incubating GEM particles with V-PA immunogen secreted in supernatant by *L. lactis* PA1001 culture (Fig. 1A–1B). To determine whether V-PA antigen was loaded on GEM particles, the assembled GEM particles presumably containing V-PA antigen were run on SDS–PAGE. The V-PA protein binding to peptidoglycan on GEM surface could be broken down by denaturing condition of SDS–PAGE and be displayed on the gel. As shown in the SDS–PAGE gel, the V-PA antigen was the major protein released from GEM particle vaccine loaded with V-PA protein (Fig. 1E), suggesting that V-PA was bound to GEM particles. To gain direct evidence that V-PA protein was loaded on GEM particle vaccine, we undertook confocal microscopy analysis. The confocal microscopy images indicated that V-PA protein, but not other control proteins, was loaded on GEM particles (Fig. 2). Flow cytometry also confirmed that V-PA was specifically loaded on GEM particles (data not shown). Therefore, V-PA protein immunogen was successfully loaded to GEM particle vaccine, and would be readily used for studies of nanostructures/single-molecule forces and immunogenicity.

3.2 The NSOM-based nanoscale characterization of V-PA immunogen loaded on GEM vaccine particles

We first tested whether some unique nanostructures of V-PA were developed on the GEM surface and whether these nanostrcutures may associate with the immunogenicity of such vaccine particles. The intrinsic ability of GEM to have thousands PA binding sites on surface may provide an excellent nanoplatform for the high-density loading of V-PA antigen [26]. Since confocal microscopy was not able to provide nanoscale-resolution images of distribution and organization of V-PA immunogen on GEM particle vaccine, the single-molecule sensitive NSOM/QD [17]-based dipole-emission fluorescence imaging system (Supporting Information Fig. S1) was employed to visualize the nanostructures and nano-organization of V-PA immunogen on GEM vaccine particle. We took advantage of the dipole emission polarization property of QDs [27] and performed 0- and 90°-polarization measurements of emitted fluorescence of QD-bound V-PA immunogens on GEM particles. The images were obtained using the PBS yielding one fluorescent image for the 0°-polarized component (left image, vertical, red color) and the other for the 90°-polarized component (right image horizontal, green color), respectively. Figures 3A and B showed a typical pair of images obtained simultaneously in the 0 and 90°-polarized emission for the QD-bound V-PA immunogen, whereas Fig. 3C was the topographic fluorescence image of V-PA imunogen loaded on surface of GEM vaccine particles.

In general, the orientation or distribution of V-PA immunogen on a GEM particle vaccine appeared randomly distributed on the GEM surface (Fig. 3D) and the mean full width at half maximum (FWHM) of fluorescent spots (Fig. 3E) was about 72.01 ± 2.81 nm (Fig. 3E). As indicated by the circled QD-bound V-PA antigen fluorescent spot (Fig. 3B), the emission variations in the relative intensities of 0- and 90°-polarized components (nothing in 0°-polarization, red color) suggested that this fluorescent spot might possess a unique emission dipole. Importantly, this allowed us to distinguish the single individual QD-bound V-PA from more advanced V-PA structures on a GEM particle. To make a more definitive assessment of the nanoscale distribution of V-PA antigen, we analyzed the colocalization degree of 0- and 90°-polarized components, which is related to the fraction of single QD or QD nanoclusters containing two or multiple QDs in the total fluorescent spots on the GEM particles. It is worth to note that as much as of 90% fluorescent spots displayed colocalization of two or multiple emission dipoles (Yellow fluorescent spots in Fig. 3D) and about 10% of fluorescent spots

NIH-PA Author Manuscript

NIH-PA Author Manuscript

NIH-PA Author Manuscript

displayed as unique emission dipole, as indicated by circled green color spot in Fig. 3B. We also analyzed the fluorescent intensity of the fluorescent spots (Fig. 3F). As shown by Fig. 3F, the spot intensities range from less than 50 to 1600 kcounts/s, suggesting the large spread in the number of QDs *per* fluorescent spot. The fluorescent spots with fluorescent intensity less than 50 Kcounts/s should correspond to single QD. Given that the total photon count rate from a fluorescent spot was directly related to the number of QDs and thus to the number of V-PA immunogen molecules, the fluorescent intensity of single QD was used to normalize the total intensity distribution and determine the number of QDs in each fluorescent spot. As shown in Fig. 3F, the overall intensity distribution indicated ~90% of fluorescent spots with intensity larger than 50 Kcounts/s should correspond to nanoclusters of QD-bound V-PA immunogen with two or multiple V-PA immunogen molecules (Fig. 3F), suggesting the multimerization rather than monomer nature of V-PA immunogen molecules on the GEM surface. Importantly, while single immunogen molecule may be enough to be recognized by B-cell receptors, multimerization nature of immunogen molecules may be one of key features of a highly immunogenic vaccine particles since it may facilitate the antigen recognition by B-cell receptors [1,28,29].

To further study the nanoscale organization of V-PA antigen in detail, we sought to quantitatively estimate the density of the V-PA immunogen on the GEM surface. The statistic analyses of fluorescence spot number suggested that there was about 1500 QD fluorescence spots on single GEM particle surface (Figs. 3A and B). Most of fluorescent spots were estimated to represent at least two QDs, as indicated by the fluorescence intensity (Fig. 3F) and colocalization analyses. Based on the conservative assumption that QD/V-PA antigen ratio is 1:1 [30, 31], it was reasonable to estimate that there were at least ~3000 QD-bound V-PA immunogen molecules on a single GEM particle. To evaluate the extent to which numbers of V-PA antigen proteins were loaded on the GEM surface, we compared the packing density of V-PA immunogen on the GEM surface with high-density CD4 molecules on T-cells. The density of V-PA immunogen estimated by NSOM/QD-based imaging was ~1492 molecules/μm^2 (based on the estimation that the diameter of GEM is 800 nm), which is much higher than the density of ~866 CD4 molecules/μm^2 (based on the estimation that the diameter of resting T-cells is 6 μm) on a CD4+ T-cell (~98 000 CD4 molecules on a single CD4+ T-cell [32]). The NSOM-based imaging may underestimate numbers of QD-bound V-PA molecules on a GEM particle, given the possibility that the relatively large QDs may block immune staining of a couple neighboring V-PA molecules, and that a QD: V-PA = 1:2 binding mode might occur somehow. Thus, the NSOM/QD-based nanoscale proteomic analysis would not overestimate V-PA immunogen loading, but allows us to conclude that high-density V-PA immunogen nanoclusters were loaded on the surface of GEM vaccine particle. It is also worth to point out that high-density of immunogen nanoclusters loaded on particle surface may be one of the important immune features of a highly immunogenic particle vaccine as a large amount of immunogen could be readily exposed to the immune system for eliciting robust immune responses [33, 34].

3.3 The AFM-based single-molecule force binding basis of V-PA immunogen loaded on GEM vaccine particles

Another key aspect for a successful particle vaccine may require that immunogens should be specifically and stably loaded on particles. While high-density loading of immunogens on particles would allow the maximum exposure of antigen protein to the immune system, it is important to note that instability and unspecific loading of immunogens on a particle has proven to be two major problems in particle vaccine development [33,35]. The possibility that the single-molecule force bases for the ability of V-PA antigen to bind to vaccine particle specifically and stably cannot be elucidated by traditional biochemical and immunologic approaches. Thus, we took advantage of AFM-based single-molecule force spectroscopy to

NIH-PA Author Manuscript

NIH-PA Author Manuscript

NIH-PA Author Manuscript

determine the nature of molecular interface between V-PA immunogen and a GEM particle. Since the round-shaped particles and microbial cells were very difficult to immobilize on substrate in buffer for AFM images, we applied polycarbonate filter membrane with a pore diameter very close to the diameter of GEM or untreated *L. lactis* cells to trap the GEM and untreated *L. lactis* cells with minimum denaturing of the cell [36]. As shown in Figs. 4A and B, a round-shaped protrusion of GEM and *L. lactis* cells could be clearly observed on the polycarbonate filter membrane. After initial AFM imaging of the surface, individual particles or cells were selected for F-D measurement to test the adhesive ability of antigen proteins to GEM or *L. lactis* cells which were firmly immobilized on substrate.

To assess the single-molecule force bases underlying the specific loading or binding between V-PA and GEM particle, HSP-functionalized AFM tips were used as control to probe GEM surface. As shown by Figs. 4D and E, almost no significant binding event between GEM and HSP was observed when HSP-functionalized AFM tips were used, indicating that HSP itself had no or very weak interaction with GEM particles. As another control, the V only protein without fusion with PA (Fig. 1) were expressed and purified, functionalized on AFM tip, and then assessed for its ability to bind to GEM. As shown by Fig. 4F, in the absence of PA, V-functionalized AFM tips shows no significant interaction with GEM when the experiments were conducted under the conditions identical to those for V-PA -functionalized AFM tips, suggesting that no specific loading or binding event could be achieved using V only protein without fusing with PA. Data based on confocal microscopy (Fig. 2), flow cytometry (data not shown), and NSOM (data not shown) also indicated that V only protein (without PA) was unable to load onto GEM. Furthermore, no significant binding between V-PA and untreated *L. lactis* cells trapped on polycarbonate membrane was observed and, in fact, untreated *L. lactis* cells showed few amount of antigen loading sites (AFM data not shown). This was consistent with data from confocal microscopy in Fig. 2, flow cytometry (data not shown), and NSOM (data not shown). In contrast, strong binding affinity of V-PA to GEM particle was demonstrated when V-PA-functionalized AFM tips were used, indicating that PA was critical to specifically load V antigen protein onto GEM. These data, again, suggested that V-PA could be specifically loaded onto GEM rather than nonspecific accumulation or absorption, which may usually catalyze protein unfolding and aggregation and therefore, reduce the corresponding immunogenicity of particle vaccines [35].

Figure 4G showed a representative F-D curve for approach and retraction of a V-PA-functionalized AFM tips from a GEM surface. It is worth to note that the essential features of the F-D curves were observed repeatedly during multiple pull-off experiments performed with the same tips, indicating that the interaction between V-PA and the GEM surface could be repeatedly rebound and repulled. The reproducible nature of the interaction between a single V-PA molecule and the GEM surface allowed us to construct a histogram of unbinding forces extracted from many F-D curves (Fig. 4G). The histogram suggested that the binding force between V-PA and GEM at physiological pH was about 51.33 ± 5.78 pN. Surprisingly, under the identical condition of AFM-based single-molecule force measurement, this V-PA antigen loading or binding force was significantly larger ($p<0.05$) than specific interaction force between HIV gp120 and CD4 (about 42.25 ± 34.14 pN, Chen Unpublished data) which plays a central role governing the HIV entry, suggesting that GEM particle has remarkably high affinity at physiological pH for loading V-PA immunogen. The strong binding force between V-PA and GEM allowed us to conclude that this GEM-based antigen protein loading system is indeed highly stable.

From the immunological standpoint, V immunogen loaded on GEM particles should be released readily from GEM for antigen processing and presentation in antigen-presenting cells after vaccination. To test the immunological pH-responsive potential of such V-PA immunogen loaded on GEM particle, we mimicked the change in environmental pH during

NIH-PA Author Manuscript

NIH-PA Author Manuscript

NIH-PA Author Manuscript

actual phagocytosis by adjusting the pH for AFM-based measurement of single-molecule force between V-PA and GEM to the range of the pH in the phagolysosome (*e.g.*, pH = 4.4). The acidic pH in the phagolysosomes is essential for processing of protein antigen to small peptides for antigen presentation. Interestingly, almost no interaction force between V-PA and GEM was observed at this acidic pH, as shown by Fig. 4D. The binding probability (the percentage for the observable specific interaction between V-PA and GEM) between V-PA-functionalized AFM tips and GEM particles decreased to the range lower than 10% (Fig. 4H), implying that V-PA would be released readily from GEM particles after acidification during phagocytosis. The abrogation of atomic force binding of V-PA to GEM could be explained by the fact that the V-PA immungen molecules at the pH 4.4 that is lower than the isoelectric point of V-PA can become net positive charge molecules from originally negative charge at the physiological pH 7.2 in which V-PA is loaded onto the surface of GEM particles. Such changes in charges of V-PA would certainly lead to the abrogation of interaction between V-PA and GEM under the phagolysosomal acidic pH. In fact, the X-ray crystallography [37] analysis of PA underscores the importance of conserved negative charge amino acids of PA for the binding to the GEM particles. Collectively, these pieces of data demonstrate that while V-PA immunogen loaded physically on GEM particle surface is highly stable and specific, the vaccine particles are immunologically pH-responsive for releasing V immunogen for antigen processing and presentation in acidic pH in the phagolysosomes of antigen presenting cells.

3.4 Immunogenicity of V-PA immunogen loaded on GEM vaccine particles

Given the high-density, high-stability, specific, and pH-responsive loading of V-PA nanoclusters on GEM particle vaccine, we then asked whether such vaccine particle could elicit robust immune responses *in vivo*. We focused on V immunogen-specific antibody responses since anti-V antibody could confer immune protection against *Y. pestis* challenge [8]. Thus, five mice were intranasally immunized with these GEM particles loaded with high density of V-PA nanoclusters at weeks zero, four, and eight (Fig. 5A), and then assessed for the development of anti-V antibody responses in serum using ELISA. The mice immunized with the GEM particle vaccine loaded with high density of V-PA nanoclusters developed robust anti-V IgG antibody responses whereas almost no anti-V IgG antibody responses were detected in mice that were vaccinated with V immunogen only (data not shown here) or GEM without loading V-PA immunogen ($p<0.05$) (Fig. 5B). These results suggested that high-density, high-stability, and pH-responsive loading of individual V-PA immunogen and V-PA nanoclusters on GEM vaccine particle could readily be delivered to the immune system for induction of strong V antigen-specific immune responses.

4 Concluding remarks

Our NSOM/QD-based proteomics shows a high-density distribution of V-PA nanoclusters on GEM vaccine particle. AFM-based single-molecule force measurement implicates the high-stability, specific, and pH-responsive loading of V-PA immunogen on GEM vaccine particle. Intranasal vaccination of mice suggested that such high-density, high-stability, specific, and pH-responsive loading of V-PA nanoclusters on GEM vaccine particle could induce robust antigen-specific immune response. The combined NSOM/AFM nanotechnology provides new insights into proteomic aspects of vaccine development.

Supplementary Material

Refer to Web version on PubMed Central for supplementary material.

NIH-PA Author Manuscript

NIH-PA Author Manuscript

NIH-PA Author Manuscript

Acknowledgments

We thank Dr. K. Leenhouts for providing plasmids and L. lactis strains, Dr. Y. Dufrene for cell and particle immobilization discussions, and technique assistances from other members of the Chen lab. This work was supported by the National Institutes of Health R01 grants: HL64560 (to ZWC), RR13601 (to ZWC), and U01 grant: AI070426 (to ZWC).

Abbreviations

AFM
atomic force microscopy

DD
double deionized

FPLC
fast protein liquid chromatography

F-D
force-distance

FWHM
full width at half maximum

GEM
gram positive enhancer matrix

L. lactis
Lactococcus lactis

NSOM
near-field scanning optical microscopy

PA
protein anchor

QD
quantum dot

V-PA
V antigen-PA fusion protein

Y. pestis
Yersinia pestis

References

1. O'Hagan DT, Valiante NM. Recent advances in the discovery and delivery of vaccine adjuvants. Nat Rev Drug Discov 2003;2:727–735. [PubMed: 12951579]
2. Kwon YJ, James E, Shastri N, Frechet JM. *In vivo* targeting of dendritic cells for activation of cellular immunity using vaccine carriers based on pH-responsive micro-particles. Proc Natl Acad Sci USA 2005;102:18264–18268. [PubMed: 16344458]
3. Reddy ST, van der Vlies AJ, Simeoni E, Angeli V, et al. Exploiting lymphatic transport and complement activation in nanoparticle vaccines. Nat Biotechnol 2007;25:1159–1164. [PubMed: 17873867]
4. Ivanov YD, Govorun VM, Bykov VA, Archakov AI. Nanotechnologies in proteomics. Proteomics 2006;6:1399–1414. [PubMed: 16447155]
5. Johnson CJ, Zhukovsky N, Cass AE, Nagy JM. Proteomics, nanotechnology and molecular diagnostics. Proteomics 2008;8:715–730. [PubMed: 18297650]

NIH-PA Author Manuscript

NIH-PA Author Manuscript

NIH-PA Author Manuscript

6. Bosma T, Kanninga R, Neef J, Audouy SA, et al. Novel surface display system for proteins on nongenetically modified Gram-positive bacteria. Appl Environ Microbiol 2006;72:880–889. [PubMed: 16391130]
7. Cornelis GR, Boland A, Boyd AP, Geuijen C, et al. The virulence plasmid of *Yersinia*, an antihost genome. Microbiol Mol Biol Rev 1998;62:1315–1352. [PubMed: 9841674]
8. Glynn A, Roy CJ, Powell BS, Adamovicz JJ, et al. Protection against aerosolized *Yersinia pestis* challenge following homologous and heterologous prime-boost with recombinant plague antigens. Infect Immun 2005;73:5256–5261. [PubMed: 16041052]
9. Griffin K, Bedford R, Townson K, Phillpotts R, et al. Protective efficacy of a recombinant plague vaccine when co-administered with another sub-unit or live attenuated vaccine. FEMS Immunol Med Microbiol 2005;43:425–430. [PubMed: 15708318]
10. Chen Y, Cai J, Xu Q, Chen ZW. Atomic force bio-analytics of polymerization and aggregation of phycoerythrin-conjugated immunoglobulin G molecules. Mol Immunol 2004;41:1247–1252. [PubMed: 15482861]
11. Chen Y, Wu Y, Cai J. Atomic force microscopic investigation on the potential early intermediate stages of fibrillo-genesis of fibronectin within fibrils. Biochem Biophys Res Commun 2007;361:391–397. [PubMed: 17645869]
12. Kuznetsov VY, Ivanov YD, Archakov AI. Atomic force microscopy revelation of molecular complexes in the multi-protein cytochrome P450 2B4-containing system. Proteomics 2004;4:2390–2396. [PubMed: 15274134]
13. Zeng G, Yang P, Zheng Z, Feng Q, et al. Nanostructures and molecular force bases of a highly sensitive capacitive immunosensor. Proteomics 2005;5:4347–4353. [PubMed: 16294312]
14. Oberhauser AF, Carrion-Vazquez M. Mechanical biochemistry of proteins one molecule at a time. J Biol Chem 2008;283:6617–6621. [PubMed: 18195002]
15. Ianoul A, Grant DD, Rouleau Y, Bani-Yaghoub M, et al. Imaging nanometer domains of beta-adrenergic receptor complexes on the surface of cardiac myocytes. Nat Chem Biol 2005;1:196–202. [PubMed: 16408035]
16. de Bakker BI, de Lange F, Cambi A, Korterik JP, et al. Nanoscale organization of the pathogen receptor DC-SIGN mapped by single-molecule high-resolution fluorescence microscopy. Chemphyschem 2007;8:1473–1480. [PubMed: 17577901]
17. Chen Y, Shao L, Ali Z, Cai J, et al. NSOM/QD-based nanoscale immunofluorescence imaging of antigen-specific T-cell receptor responses during an *in vivo* clonal V{gamma}2 V{delta}2 T-cell expansion. Blood 2008;111:4220–4232. [PubMed: 18039956]
18. Lewis A, Taha H, Strinkovski A, Manevitch A, et al. Near-field optics: From subwavelength illumination to nanometric shadowing. Nat Biotechnol 2003;21:1378–1386. [PubMed: 14595366]
19. Tokumasu F, Hwang J, Dvorak JA. Heterogeneous molecular distribution in supported multicomponent lipid bilayers. Langmuir 2004;20:614–618. [PubMed: 15773083]
20. Dunn RC. Near-field scanning optical microscopy. Chemical Reviews 1999;99:2891. [PubMed: 11749505]
21. Brehm M, Taubner T, Hillenbrand R, Keilmann F. Infrared spectroscopic mapping of single nanoparticles and viruses at nanoscale resolution. Nano Lett 2006;6:1307–1310. [PubMed: 16834401]
22. Chen Y, Qin J, Chen ZW. Fluorescence-topographic NSOM directly visualizes peak-valley polarities of GM1/GM3 rafts in membrane fluctuations. J Lipid Res 2008;49:2268–2275. [PubMed: 18603643]
23. Chen Y, Cai J, Zhao T, Wang C, et al. Atomic force microscopy imaging and 3-D reconstructions of serial thin sections of a single cell and its interior structures. Ultra-microscopy 2005;103:173–182.
24. de Bakker BI, Bodnar A, van Dijk EM, Vamosi G, et al. Nanometer-scale organization of the alpha subunits of the receptors for IL2 and IL15 in human T lymphoma cells. J Cell Sci 2008;121:627–633. [PubMed: 18287585]
25. Shen Y, Zhou D, Qiu L, Lai X, et al. Adaptive immune response of $V\gamma 2V\delta 2^{+}$ T cells during mycobacterial infections. Science 2002;295:2255–2258. [PubMed: 11910108]
26. Steen A, Buist G, Leenhouts KJ, El Khattabi M, et al. Cell wall attachment of a widely distributed peptidoglycan binding domain is hindered by cell wall constituents. J Biol Chem 2003;278:23874–23881. [PubMed: 12684515]

NIH-PA Author Manuscript

NIH-PA Author Manuscript

NIH-PA Author Manuscript

27. Empedocles SA, Neuhauser R, Bawendi MG. Three-dimensional orientation measurements of symmetric single chromophores using polarization microscopy. Nature 1999;399:126–130.
28. Bachmann MF, Rohrer UH, Kundig TM, Burki K, et al. The influence of antigen organization on B cell responsiveness. Science 1993;262:1448–1451. [PubMed: 8248784]
29. Bernasconi NL, Traggiai E, Lanzavecchia A. Maintenance of serological memory by polyclonal activation of human memory B cells. Science 2002;298:2199–2202. [PubMed: 12481138]
30. Wang H, Tessmer I, Croteau DL, Erie DA, et al. Functional characterization and atomic force microscopy of a DNA repair protein conjugated to a quantum dot. Nano Lett 2008;8:1631–1637. [PubMed: 18444686]
31. Pathak S, Davidson MC, Silva GA. Characterization of the functional binding properties of antibody conjugated quantum dots. Nano Lett 2007;7:1839–1845. [PubMed: 17536868]
32. Davis KA, Abrams B, Iyer SB, Hoffman RA, et al. Determination of CD4 antigen density on cells: Role of antibody valency, avidity, clones, and conjugation. Cytometry 1998;33:197–205. [PubMed: 9773880]
33. Neutra MR, Kozlowski PA. Mucosal vaccines: The promise and the challenge. Nat Rev Immunol 2006;6:148–158. [PubMed: 16491139]
34. St Clair N, Shenoy B, Jacob LD, Margolin AL. Cross-linked protein crystals for vaccine delivery. Proc Natl Acad Sci USA 1999;96:9469–9474. [PubMed: 10449716]
35. Zhu G, Mallery SR, Schwendeman SP. Stabilization of proteins encapsulated in injectable poly (lactide- co-glycolide). Nat Biotechnol 2000;18:52–57. [PubMed: 10625391]
36. Dupres V, Menozzi FD, Locht C, Clare BH, et al. Nanoscale mapping and functional analysis of individual adhesins on living bacteria. Nat Methods 2005;2:515–520. [PubMed: 15973422]
37. Bateman A, Bycroft M. The structure of a LysM domain from *E. coli* membrane-bound lytic murein transglycosylase D (MltD). J Mol Biol 2000;299:1113–1119. [PubMed: 10843862]

NIH-PA Author Manuscript

NIH-PA Author Manuscript

NIH-PA Author Manuscript

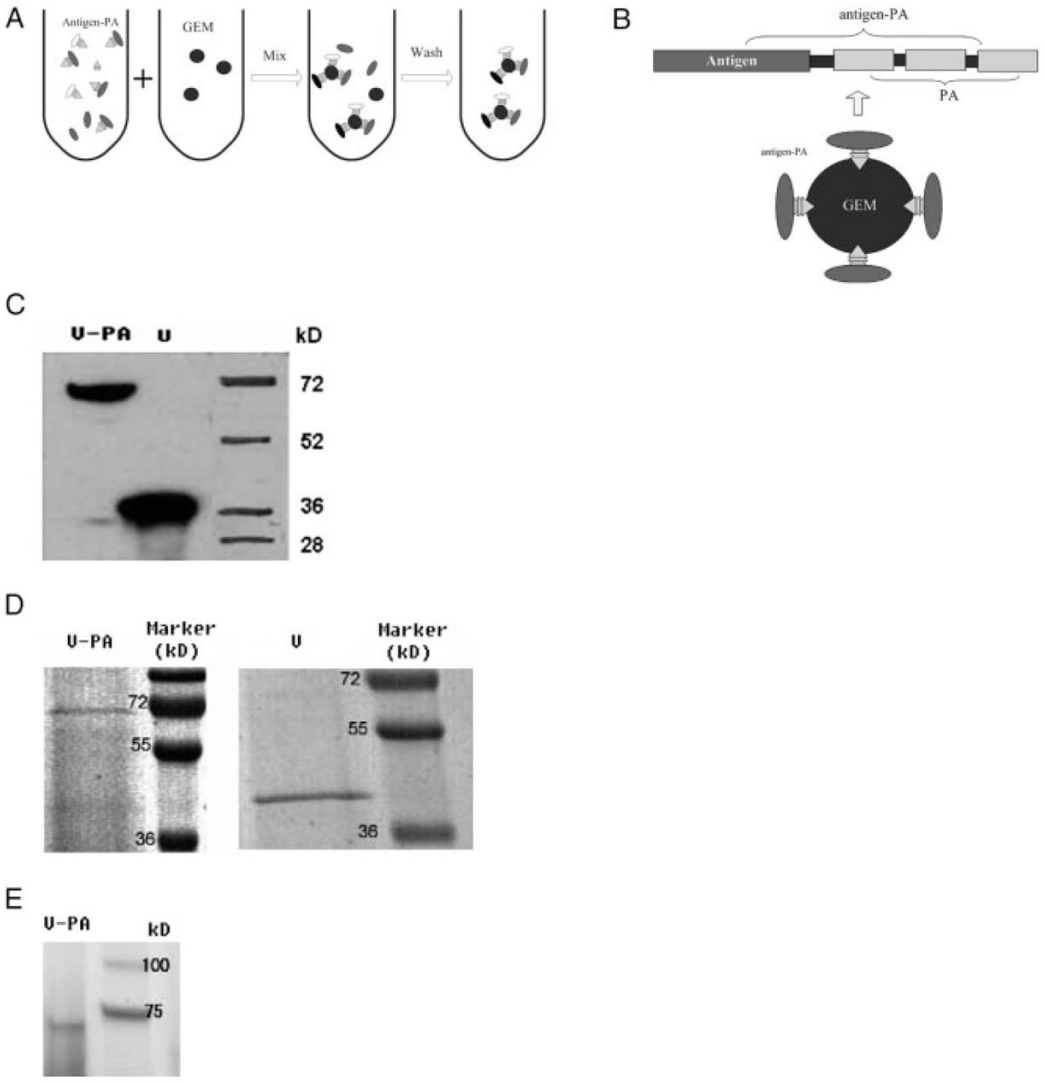

Figure 1.

Biochemical characterization of the loading of V-PA immunogen on GEM vaccine particle. (A) A scheme showing the loading of *Y. pestis* V-PA immunogen on GEM vaccine particles. GEM particles were derived from pretreated *L. lactis* as described in Section 2 and Supporting Information. Drawings are not scaled. V-PA antigen in culture supernatant was incubated with GEM particles in for 1 h at room temperature, followed by thoroughly washing to remove unbound antigens. (B) A scheme showing an assembled GEM containing V-PA antigen proteins. Drawings are not scaled. (C) Western blot demonstrated that mAb against c-Myc present as tag in expressed protein identified V and PA fusion protein (V-PA) and V only protein secreted in culture supernatant by recombinant *L. lactis* expressing V-PA and V, respectively. (D) SDS–PAGE showing V-PA (left) and V proteins (right) purified by fast protein LC (FPLC). (E) SDS–PAGE gel analysis indicated that the assembled GEM particle vaccine contained V-PA protein. V-PA antigen was first loaded onto GEM as described in Fig. 1(A); the assembled GEM particles were then run on SDS–PAGE gel in the gel-loading buffer.

NIH-PA Author Manuscript
NIH-PA Author Manuscript
NIH-PA Author Manuscript

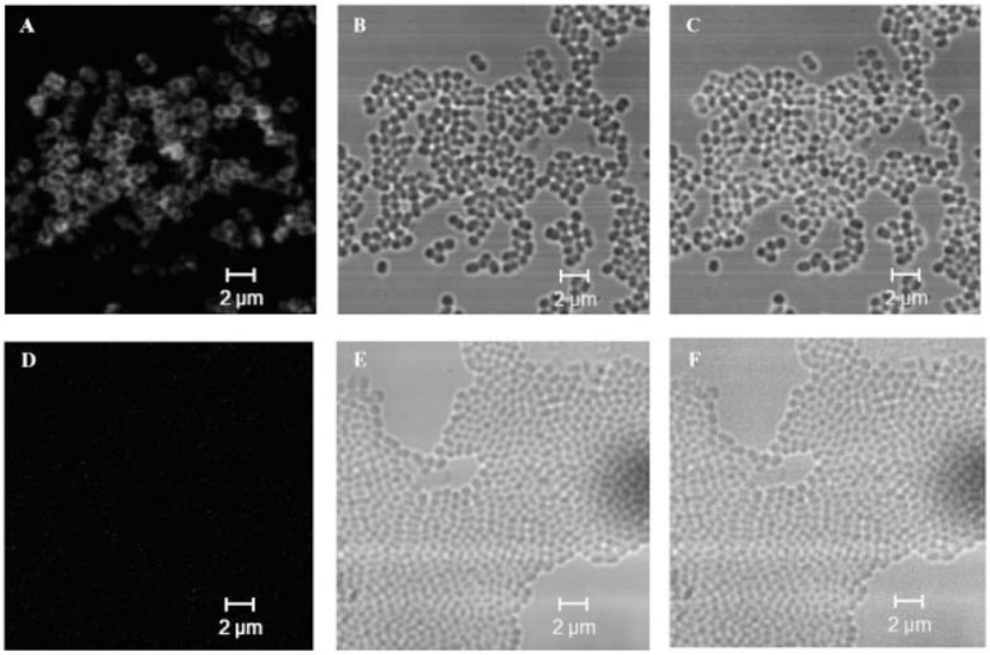

Figure 2.

Representative confoal microscopy images showing that V-PA immunogen was loaded on GEM vaccine particle. Staining was done using anti-c-Myc mAb and QD-conjugated antimouse IgG as described in Section 2 and Supporting Information. (A), (B), and (C) are fluorescent, DIC, and merged fluorescent- differential interference contrast (DIC) images, respectively for GEM particle vaccine containing V-PA antigen. (D), (E), and (F) are fluorescent, DIC, and merged fluorescent-DIC images, respectively, for the control sample, GEM particles incubated with *Y. pestis* V antigen without PA, respectively. No fluorescence was observed for another control, GEM particles incubated with PBS (data not shown).

NIH-PA Author Manuscript

NIH-PA Author Manuscript

NIH-PA Author Manuscript

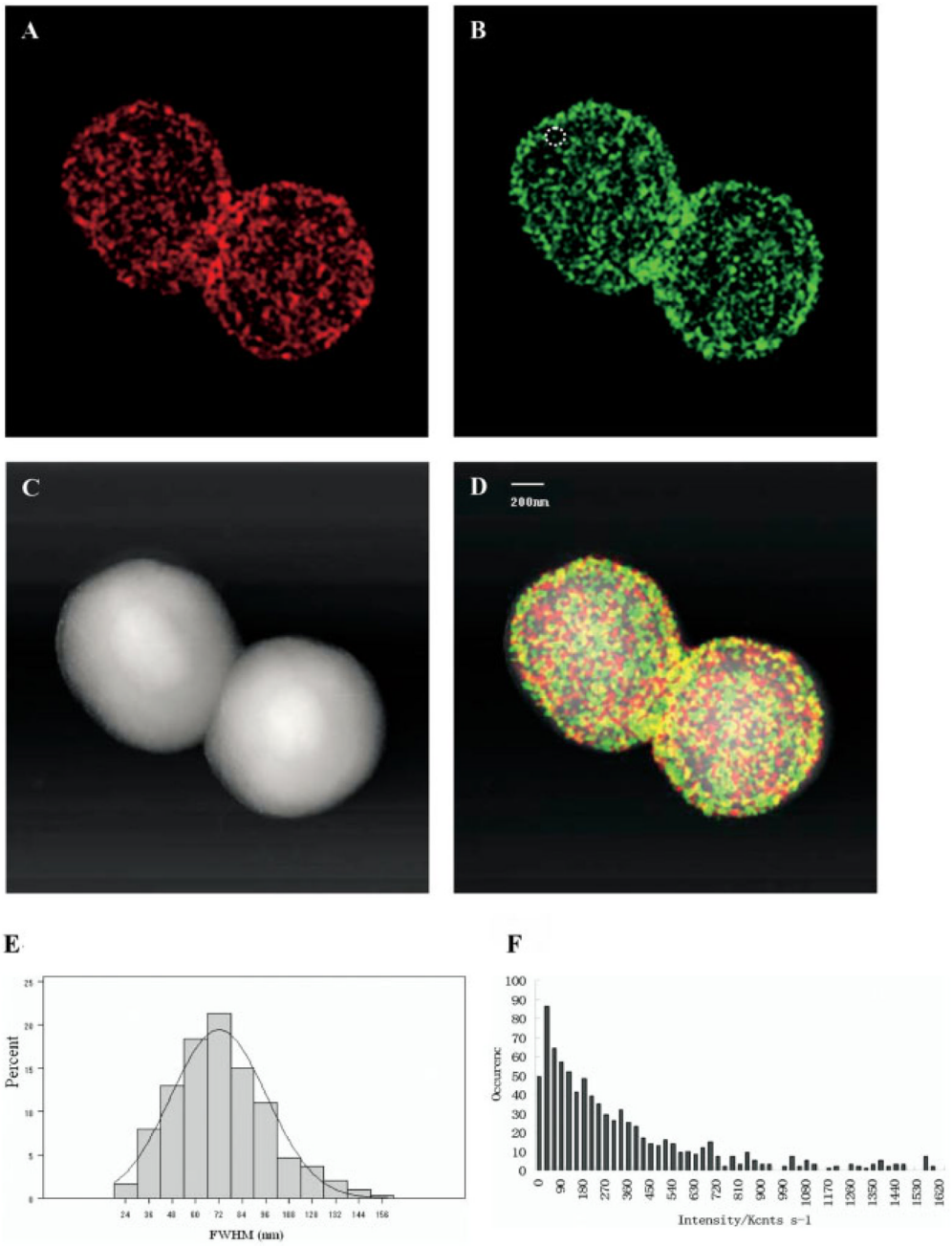

Figure 3.

NSOM/QD-based proteomics shows that majority of V-PA antigen molecules were packed as nanoclusters on the surface of GEM vaccine particle. At least ten individual GEM particles loading V-PA immunogen were imaged for analyses. Figures 3A and B show that the 0 *versus* 90° split emission images for QD-bound V-PA antigen on the surface of GEM particle vaccine were acquired simultaneously by NSOM, showing the vertical polarization component (0°, 3A) and the horizontal component (90°, 3B). Figure 3C shows the topographic imaging of a GEM particle loading V-PA antigen. Figure 3D is a merged topographic (C) and fluorescent (Figs. 3A and B) image. In both (A) and (B), the fluorescence signal is color-coded based on the detected polarization. Individual single-QD-bound V-PA antigen molecules are

NIH-PA Author Manuscript

NIH-PA Author Manuscript

NIH-PA Author Manuscript

determined by their unique vertical (A) or horizontal (B) only dipole emission, as shown by the circled fluorescent spot in (B). The yellow color of fluorescent spots results from accumulated emission of multiple clustered molecules with random in-plane orientation (merging of red and green) in one fluorescent spot. (E) is the histogram of FWHM of fluorescent spots. (F) is the histogram for the intensity distribution of all measured fluorescent spots. No fluorescence was observed on GEM particles incubated with PBS only or with V antigen only (without fusing PA) (data not shown here).

NIH-PA Author Manuscript

NIH-PA Author Manuscript

NIH-PA Author Manuscript

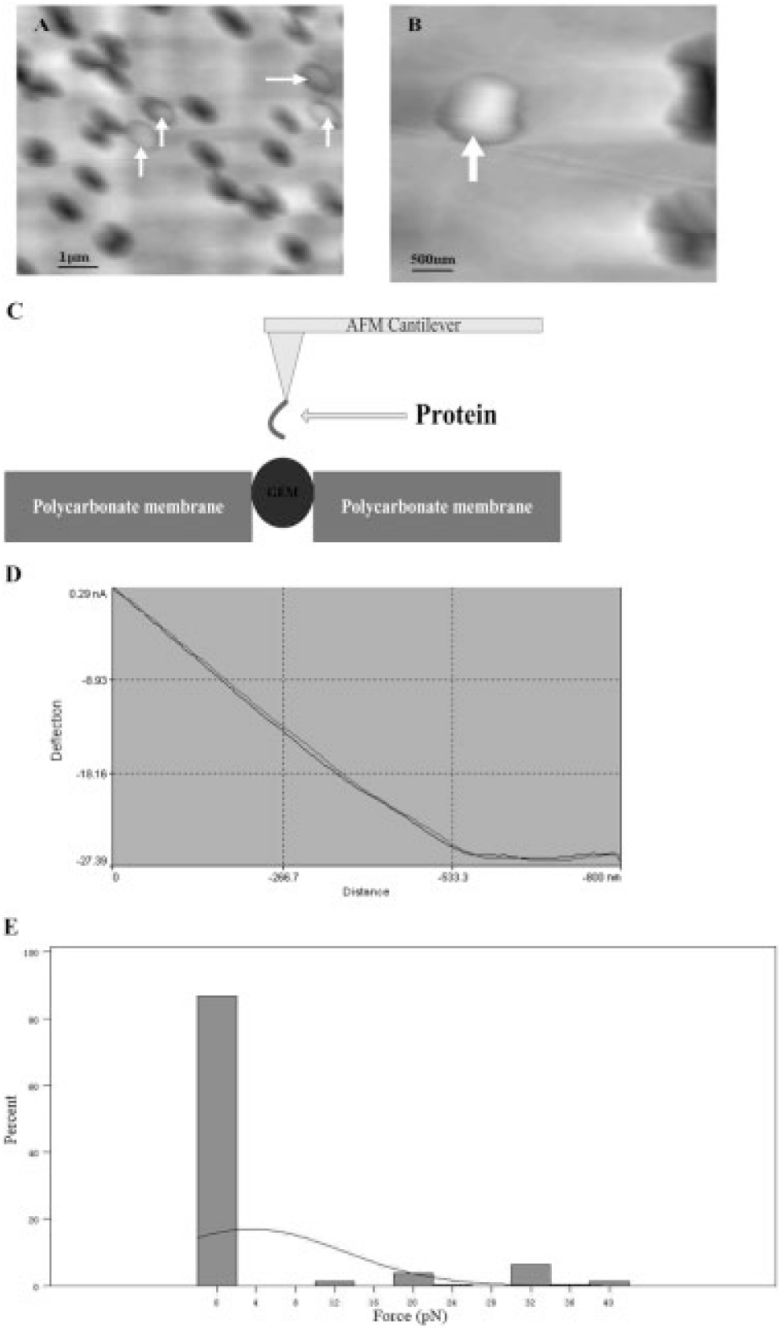

NIH-PA Author Manuscript

NIH-PA Author Manuscript

NIH-PA Author Manuscript

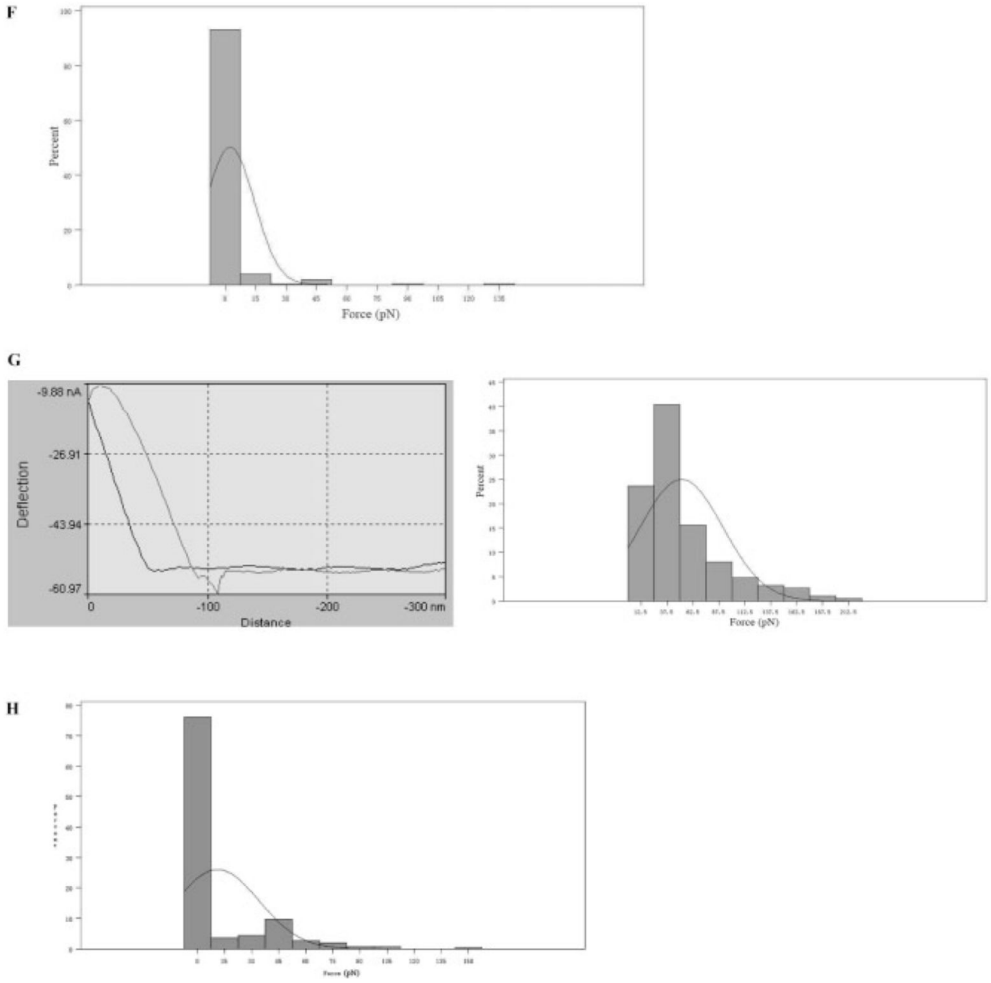

Figure 4.

AFM-based single-molecule binding features of potential V-PA immunogen loading. (A) A representative AFM topographic image showing four single GEM particles trapped in filter membrane. (B) A representative AFM topographic image showing a single GEM particle trapped in filter membrane. (C) Experiment design for measuring the atomic force between V-PA and surface peptidoglycan of a GEM particle. (D) A representative force-distance curve showing no interaction between functionalized HSP and the GEM particle. (E) A representative histogram showing no biding force between the functionalized HSP and the GEM particle in PBS buffer (pH 7.4, NaCl 137 mM). $N = 300$. Similar results were observed in at least three independent experiments. (F) A representative histogram showing no binding force between the V antigen-functionalized AFM tips and the GEM particle in PBS buffer (pH 7.4, NaCl 137 mM). $N = 300$. At least three independent experiments were performed. (G) Representative F-D curve and histogram showing the binding atomic force between the V-PA-functionalized AFM tips and the GEM particle in PBS buffer (pH 7.4, NaCl 137 mM). $N = 300$. Similar results were observed in at least three independent experiments. (H) Histogram for the interaction forces between V-PA and GEM particles under buffer at the range of low phagolysosomal pH (=4.4) and NaCl 137 mM. $N = 300$. The binding between V-PA and GEM particles abrogated significantly under this pH.

NIH-PA Author Manuscript

NIH-PA Author Manuscript

NIH-PA Author Manuscript

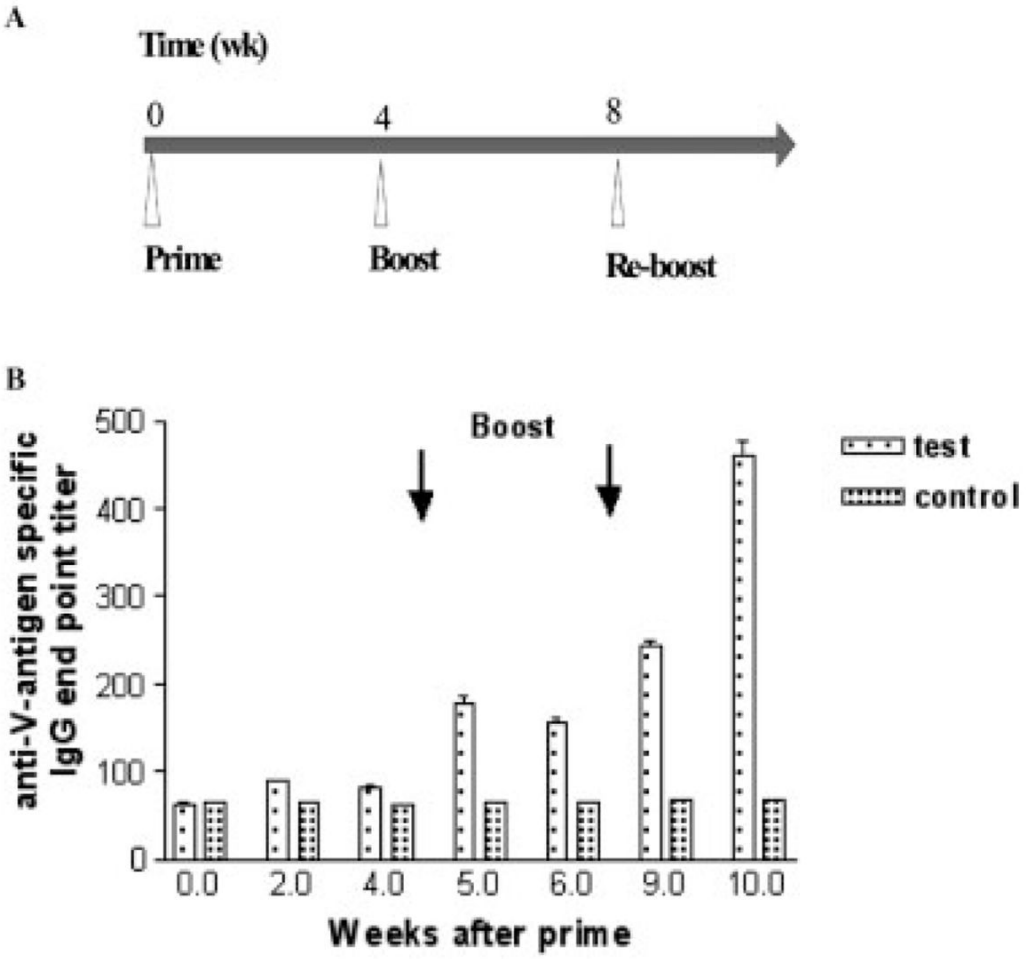

Figure 5.

Intranasal vaccination of mice with V-PA nanoclusters-containing GEM vaccine particle elicited high-level V-specific antibody responses. (A) The scheme showing the time course of vaccination with GEM particle without V-PA antigen (control group), GEM particle containing V-PA antigen (test group) (B) Anti-V specific IgG antibody end point titers in mice vaccinated with GEM without V-PA antigen (control group) or GEM particle containing V-PA antigen (test group). Antibody titers were determined by ELISA as described in Section 2.